Politecnico di Torino

Université Paris Cité

Double Degree in
Nanotechnologies for ICTs and Quantum Devices

INTERNSHIP REPORT

Magneto-ionic control of 90° domain walls for neuromorphic computing

Candidate:
Claudia Tataru

Internship supervisor:
Dr. Liza Herrera Diez

Academic supervisors:
Prof. Maria Luisa Della Rocca
Prof. Carlo Ricciardi

Academic Year 2023-2024

C2N CENTRE DE NANOSCIENCES ET DE NANOTECHNOLOGIES

cnrs université PARIS-SACLAY

Contents

Chapter 1

Introduction

The internship has been carried out at the *Centre for Nanoscience and Nanotechnology* (C2N), in the group *Integnano* (INTEGrative concepts for spin and charge based NANOdevices). The research team gathers interdisciplinary expertise in different aspects of spintronics and neuromorphic computing architectures. In particular, the subgroup I worked with has been at the forefront of investigating the magneto-ionic control of magnetic anisotropy, magnetic domain wall motion, and the Dzyaloshinskii-Moriya interaction in different materials. The non-volatility, reversibility and large amplitude of the gating effects is what makes magneto-ionics particularly attractive for spintronics applications, where dynamic reconfiguration of magnetic properties is highly sought after. On the other hand, magneto-ionics integrates the concept of voltage-driven ionic motion from memristor technologies, commonly used in neuromorphic applications, with spintronics. This combination provides a promising avenue for the development of novel neuromorphic functionalities based on spintronic devices.

In this context, the research project I took part in aims at designing artificial synaptic functionalities in magneto-ionic gating devices for neuromorphic computing. Magneto-ionics provides both binary states given by the two magnetization orientations in ferromagnets with perpendicular magnetic anisotropy and analog states given by its ionic control of magnetic anisotropy. The binary states can emulate plasticity in binary neural networks by changing synaptic weights, while the ionic states can emulate metaplasticity, allowing for sequential learning without memory loss, i.e. learning a new task without forgetting the previously learned one, like in the human brain. The latter is a feature based on assigning a 'hidden value' to each synaptic state to encode how important each state is. This establishes a hierarchy among synaptic values, making 'strong' states difficult to forget (high anisotropy) and 'weak' states easy to forget (Figure 1.1). Hence, an in-depth study of the physics of magneto-ionic nanodevices and the dynamics of the voltage-induced anisotropy changes is crucial to design synaptic devices.

The main objective of the internship was to investigate the dynamics of 90° domain walls between two anisotropy states, a new promising spin structure, under the application of a gate voltage in oxygen-based magneto-ionic devices. This was accomplished through

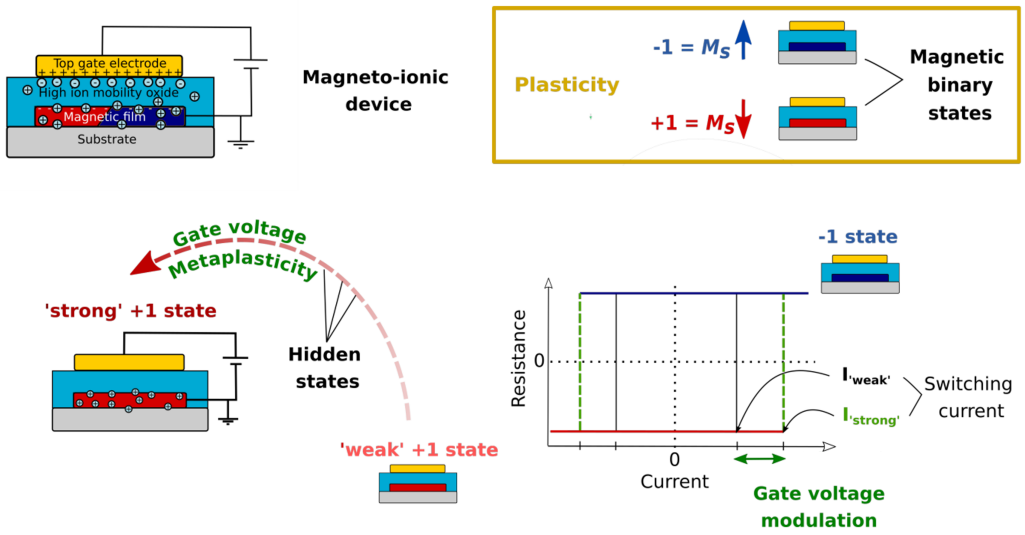

Figure 1.1: Schematic representation of the metaplastic feature introduced by the gate voltage. Magneto-ionic devices have two binary states, each can be defined as 'weak' or 'strong' (easier or harder to switch) thanks to non-volatile ionic motion (circles) under a gate voltage.

the combination of magneto-transport measurements and Kerr microscopy magnetic imaging. The report starts with fundamental theoretical concepts that present the common features between magneto-ionics and neuromorphic computing, followed by a description of the experimental techniques employed. Finally, the last part focuses on the solid-state device characterization.

Chapter 2

Theoretical background

This chapter aims at providing an overview of basic theoretical concepts linking magnetism and memristors.

2.1 Ferromagnetism and magnetic interactions

Ferromagnetic materials are a class of magnetic materials which are able to preserve a strong net alignment of magnetic moments even without the presence of an external magnetic field. Below a critical temperature (Curie temperature T_c), this alignment gives rise to a non-zero spontaneous magnetization M within the material. The magnetic configuration of a ferromagnet is determined by the competition between different fundamental interactions that contribute to the total energy of the system, described by the following equation:

$$E_{total} = E_{ex} + E_D + E_{an} + E_Z \tag{2.1}$$

where exchange, dipolar, anisotropy and Zeeman energies are involved.

- **Exchange energy**
  It is a short-range microscopic interaction between neighbouring spins which promotes magnetic ordering. This behaviour stems from the antisymmetry of the wave function describing identical fermions, implying that the total wave function must change sign when the positions of any two identical fermions are exchanged. It is represented by the Heisenberg Hamiltonian, expressed as:

  $$H = -\sum_{i<j} J_{ij} \vec{S_i} \cdot \vec{S_j} \tag{2.2}$$

  where J_{ij} is the exchange constant, while $\vec{S_i}$ and $\vec{S_j}$ are a pair of spins. A positive J leads to a ferromagnetic coupling, giving a minimum exchange energy when spins are parallel.

- **Dipolar energy**
  It is a non-local interaction between the magnetic field created by the internal

magnetic moments H_D, called demagnetizing field and the magnetization M. The magnetization discontinuity at the surface generates uncompensated "magnetic poles", giving rise to the internal H_D that tends to oppose M ($\nabla H = -\frac{1}{\mu_0}\nabla M$). The dipolar energy can be expressed as:

$$E_D = -\frac{\mu_0}{2}\iiint_V \vec{M}\cdot\vec{H}_D\, dV = -\frac{\mu_0}{2}\vec{M}\cdot(-N_D\cdot\vec{M}) \tag{2.3}$$

where μ_0 is the vacuum magnetic permeability, V is the magnetic system volume and N_D is the demagnetizing factor which accounts for the shape of the sample.
Reducing the number of magnetic dipoles at the surface and as a consequence reducing H_D results in the minimization of the dipolar energy. Hence, magnetization naturally tends to align parallel to the edges and surfaces of a material. In the case of thin films, when the magnetization forms an angle θ with the film normal, the dipolar energy assumes the following expression:

$$E_D = \frac{\mu_0}{2}M_s^2 cos^2(\theta) \tag{2.4}$$

where M_s is the saturation magnetization.

- **Anisotropy energy**
  It describes the natural tendency of the magnetization to orient along fixed directions. The main sources of anisotropy are related to the crystal structure, shape and interfaces of a magnetic material. *Magnetocrystalline anisotropy* is an intrinsic property associated with the crystal symmetry which favours the magnetization along particular crystallographic axes. The magnetization direction for which the energy is minimized is called the easy axis. On the contrary, the magnetization direction for which the energy is maximized is called the hard axis. It arises from spin-orbit interaction, which couples the spin angular momentum of an electron to its orbital angular momentum. A single easy axis leads to *uniaxial anisotropy* whose corresponding energy assumes the following form if one considers only the dominant term:

$$E_A = K_u sin^2(\alpha) \tag{2.5}$$

where K_u is the volume anisotropy constant (J/m^3) and α is the angle between the easy axis and the magnetization.
In magnetic thin films, the broken symmetry of the atoms at the interfaces introduces another term to the magnetic anisotropy, namely the *interface anisotropy energy* given by:

$$E_S = \frac{K_S}{t}sin^2(\theta) \tag{2.6}$$

where K_S is the surface anisotropy constant (J/m^3), t is the thickness of the ferromagnetic layer and θ is the angle between the magnetization and the surface normal.
In addition, non spherical magnetic materials will exhibit a *shape anisotropy* which induces the alignment of the magnetization along the long axis.

- **Zeeman energy**
  It represents the energy associated with the interaction between the magnetization and an external magnetic field H_{ext}, defined as:

$$E_Z = -\mu_0 M \cdot H_{ext} \tag{2.7}$$

  Equation 2.7 implies that Zeeman energy is minimized when M and H_{ext} are parallel.

The interplay of the interactions presented above affects the alignment of the magnetic moments in a ferromagnetic material and results in a definition of an effective magnetic anisotropy constant (K_{eff}) per unit volume, which can be expressed as:

$$K_{eff} = K_V + \frac{K_S}{t} - \frac{\mu_0 M_s^2}{2} \tag{2.8}$$

where K_V and K_S represent the volume and the surface anisotropy contributions, respectively and the last term represents the dipolar energy. The corresponding energy is $E_{an} = K_{eff}\ sin^2(\theta)$. The sign of K_{eff} determines the minimum energy configuration and thus the easy axis. When $K_{eff} < 0$, the easy axis lies in-plane ($\theta \in \{-\frac{\pi}{2}, \frac{\pi}{2}\}$). As the interface contribution becomes more dominant, K_{eff} becomes positive and the easy axis becomes perpendicular to the plane ($\theta \in \{0, \pi\}$).

2.2 Voltage control of magnetic anisotropy (VCMA)

Nowadays, one of the main challenges in magnetic memory architectures is the reduction of energy consumption. This need has driven the exploration of alternative magnetic memory designs. Notably, the energy barriers involved in the magnetic switching process can be efficiently regulated by manipulating magnetic anisotropy through electric fields. This enables dynamic switching between soft magnetic states, which are easily accessible with low energy for writing information, and hard magnetic states for reliable information retention. Unlike state-of-the-art magnetic random access memory (MRAM) technology which employs highly-dissipating current, the voltage control of magnetic anisotropy holds potential in a wide range of spintronics applications, requiring only the energy cost of charging a capacitor-like device. On a parallel line, magnetic anisotropy in thin films and multilayers has been studied for more than 60 years and is typically observed in materials with significant spin-orbit interactions like Co/Pd and Co/Pt multilayers. In particular, interfacial perpendicular anisotropy (iPMA) was discovered to exist at the interface between magnetic transition metals and oxides in 2002 [1][2]. Despite involving relatively light elements (Fe, Al, Mg, O, etc.) characterized by weak spin-orbit interactions, the amplitude of the anisotropy is comparable to that found at Co/Pt interfaces ($\sim$1.4 mJ/m^2). X-ray absorption spectroscopy (XAS) and X-ray photoelectron spectroscopy (XPS) measurements later revealed that the underlying origin was the hybridization between the oxygen and the magnetic transition metal orbitals across the interface[3]. This hybridization reduces the degeneracy of the transition metal d-orbitals, leading to the observed perpendicular anisotropy.
It is now clear that the behaviour of magnetic nanoscale devices largely depends on their

surface magnetic properties. Voltage control of magnetism can be engineered mainly through electrostatic charging or electrochemical mechanisms, including magneto-ionic effects which will be discussed in the following section.

2.3 Magneto-ionics

Magneto-ionics is an emerging field at the intersection of materials science, chemistry and magnetism, focusing on the electrical manipulation of magnetic properties mediated by ion migration. As presented in Fig.2.1a, a typical magneto-ionic structure involves the presence of a ion reservoir, usually a high ion mobility oxide (e.g. HfO_2 or GdO_x), in contact with a target magnetic transition metal. The application of a sufficiently high external voltage induces the motion of these charged ions towards or away from the magnetic film thus altering the local electronic structure and chemical environment. This results in the progressive surface oxidation or reduction of the latter, as shown in Fig. 2.1b,c. Unlike electrostatic gating involving the accumulation of charges, these induced changes can be non-volatile, persisting even after the gate voltage has been switched-off. Moreover, magneto-ionic effects are not limited to the magnetic surface but can extend beyond, enabling also the control of the bottom interface.
In this context, different systems have been explored [4] to exploit the full potential of magneto-ionics by focusing on the proper selection of the ion species involved in the redox process (e.g. O^{2-}[5],H^{+}[6], N^{2-}[7]), the heterostructures designs[8] as well as the gating technique, such as solid-state and ionic liquid gating [9]. Let us now focus on oxygen-based devices examined in this report. Previous studies from the Integnano group [10] unveiled a high degree of complexity in HfO_2 - based devices, where two distinct magneto-ionic regimes have been identified within the same device under the influence of ionic liquid gating. The hybridization at the ferromagnetic film/oxide interface has been shown to have a large impact on magnetic anisotropy. Consequently, three oxidation states can be distinguished:

- **Underoxidized state** in which the mobile oxygen ions have yet to reach the magnetic material which exhibits in-plane magnetic anisotropy (IPA).

- **Optimally oxidized state** in which the oxygen species reached the magnetic material surface, achieving an optimum surface coverage. A transition from in-plane to out-of-plane anisotropy (PMA) is observed.

- **Overoxidized state** in which the oxygen species continue to accumulate at the interface thus driving the system away from the optimum level of oxidation that maximizes PMA. This results in the transition to an in-plane state.

Regime I is characterized by the transition from IPA to PMA, showing a much faster dynamics and highly suppressed reversibility compared to regime II. On the other hand, regime II is defined by a slower yet reversible transition from PMA to IPA.

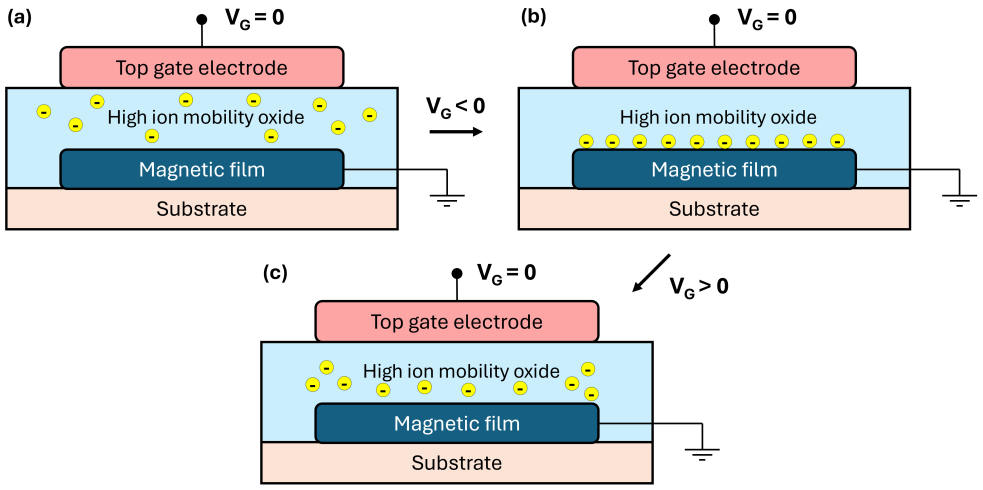

Figure 2.1: (a) Schematics of oxygen-ion-based magneto-ionic device. Depending on the applied gate voltage polarity, the O^{2-} ions (depicted as yellow circles) migrate towards or away from the magnetic layer resulting in (b) oxidation or (c) reduction, respectively.

2.4 Memristors

A memristor, short for memory resistor, is a passive two-terminal circuit element whose resistance state depends on the history of the applied voltage and current. This behavior is modeled by the non-linear relationship between charge and flux, as first predicted by Leon Chua in 1971. Its internal resistance state can be actively modulated by means of an applied voltage and retained after the voltage is turned off, making them suitable for non-volatile memory applications. Since its experimental validation in 2008 [11], many different memristive devices have been proposed and demonstrated. Among these, valence change memristors consist in an insulating oxide (e.g. HfO_2, TaO_2) sandwitched between two non-active metals. An electroforming step creates a filamentary conducting path, consisting of oxygen vacancies, within the metal oxide layer. The resistive switching mechanism, i.e. change in electrical resistance, involves the formation and rupture of the single or multiple oxygen-deficient conductive filaments under an external electric field, thereby resembling the concept of voltage-induced ion migration in magneto-ionic devices. As a key component in neuromorphic computing architectures, memristors can emulate biological synapses through their ability to change resistance in an analog manner based on past activity, enabling the replication of synaptic weight updates which are essential to the learning process. In the human brain this modulation occurs in response to the activity of the pre and post-synaptic neuron: a synapse could receive either an excitatory potential, which strengthens or increases its weight (positive stimulation), or an inhibitory potential, which weakens or decreases its weight (negative stimulation). As a result, voltage spikes arriving at the axon-end of a pre-synaptic neuron trigger the release of small molecules called neurotransmitters that flow towards the post-synaptic neuron.

Chapter 3

Experimental methods

In this chapter, the experimental techniques that were mostly employed, namely magneto-optical Kerr microscopy and magneto-transport, will be presented.

3.1 Anomalous Hall effect

In the classical Hall effect, an electric current flowing through a non-magnetic conductor generates a transverse voltage (Hall voltage), perpendicular to both the current and the vertical component of an applied magnetic field H. This phenomenon is the result of the Lorentz force $F = \mu_0 \cdot q \cdot (v \times H)$ acting on the charge carriers of charge q moving with velocity v. The Hall resistivity, defined as the ratio between the Hall voltage and the current density, increases linearly with the magnetic field. In ferromagnetic materials, however, after initially increasing with the field, it saturates to a value that is almost independent of the field. This additional contribution to the Hall resistivity, proportional to the perpendicular component of the material magnetization, is called anomalous Hall effect (AHE). Accordingly, the overall expression for the Hall resistivity is given by the following empirical relation:

$$\rho_H = R_{CHE} \cdot \mu_0 \cdot H_z + R_{AHE} \cdot \mu_0 \cdot M_z \tag{3.1}$$

where R_{CHE} and R_{AHE} are the classical Hall coefficient and anomalous Hall coefficient, respectively, μ_0 is the vacuum magnetic permeability, H_z is the out-of-plane component of the applied magnetic field and M_z is the out-of-plane component of the magnetization. In magnetic materials, R_{CHE} can be neglected as it is found to be significantly smaller than R_{AHE}. Hence, the measured Hall resistance is proportional to M_z, making AHE an efficient method to monitor the out-of-plane magnetization of a sample.
The anomalous Hall effect arises from spin-orbit coupling, which causes a deflection of charge carriers depending on their spin orientations. Although AHE is not yet fully understood, there are currently three main mechanisms that can explain its origin[12]:

(i) an intrinsic contribution associated to the electronic band structure and a spin dependent "anomalous velocity" acquired by the electrons arising from the Berry phase;

(ii) the extrinsic contributions, namely skew scattering and side jump scattering due to electron scattering with impurities.

In this report, anomalous Hall effect was used to probe the total perpendicular magnetization component of the magnetic thin film and the magnetic anisotropy.

3.2 Kerr microscopy

Kerr microscopy is a powerful technique which allows to gain insight into properties of magnetic materials, in particular the observation of magnetic microstructures changes. In this section, the magneto-optical Kerr effect and its application in the Kerr microscope will be briefly discussed.

3.2.1 Magneto-optical Kerr effect

The magneto-optical Kerr effect (MOKE) is a sensitive and non-destructive optical phenomenon which relies on the interaction between light and the magnetization within a material. When a linearly polarized light beam is reflected by a magnetized surface, it undergoes a rotation of its polarization axis θ_k and a change in ellipticity ϕ_k, becoming elliptically polarized. This occurs because the magnetization of the medium introduces an additional light oscillation component due to the Lorentz force, known as the Kerr component, which is perpendicular to the oscillations of electrons induced by the electric field of the incoming incident light. The superposition of both these oscillations results in the elliptical polarization of the reflected light.

The magneto-optical Kerr effect can be classified into three different geometries shown in Figure 3.1, each depending on the orientation of the magnetization with respect to the plane of incidence of the light and the reflecting surface:

- *Transverse MOKE* where the magnetization is parallel to the reflecting surface (M $\perp$ n) but perpendicular to the plane of incidence. It yields an amplitude variation of the incident light and no change in polarization.

- *Longitudinal MOKE* where the magnetization lies both in the plane of the reflecting surface and the plane of incidence (M $\perp$ n).

- *Polar MOKE* where the magnetization is perpendicular to the reflecting surface (M $\parallel$ n) and parallel to the plane of incidence.

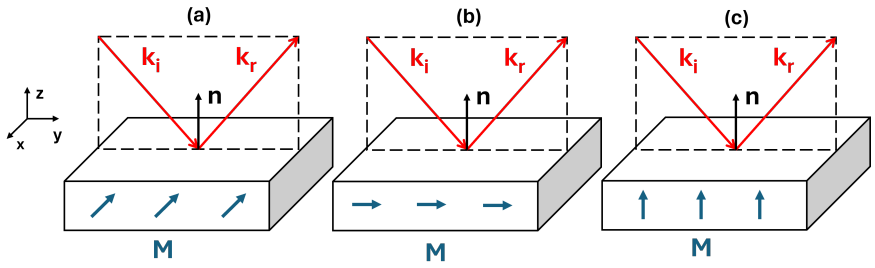

Figure 3.1: Different geometries of the magneto-optical Kerr effect. k_i and k_r are the propagation direction of the incident and reflected light beam respectively, n is the unit vector normal to the surface and M is the magnetization. (a) Transverse MOKE. (b) Longitudinal MOKE. (c) Polar MOKE.

All the magnetic images presented in this report were acquired using a Kerr microscope in the polar MOKE configuration with the incoming wave normal to the surface sample as illustrated in Figure 3.2. It is important to point out that this is the only configuration that is non-zero at normal incidence and therefore sensitive to the out-of-plane component of the magnetization.

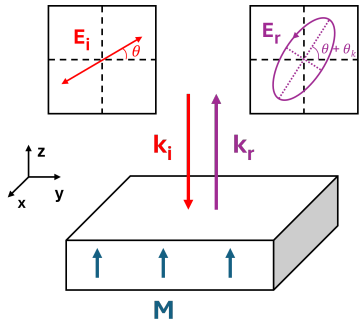

Figure 3.2: Polar MOKE with normal incidence of the incoming light. After being reflected by the perpendicular magnetized sample, the incident linearly polarized wave E_i is rotated by the Kerr angle θ_k which is proportional to the magnetization M_z and becomes elliptically polarized E_r.

3.2.2 Kerr microscope

As the name suggests, a Kerr microscope is an optical microscope that exploits MOKE to obtain images with magneto-optical contrast and whose strength lies in its ability to detect very small Kerr rotations or ellipticity in the reflected light. A red LED with a wavelength $\lambda = 630$ nm was chosen as the light source to illuminate the sample. Figure 3.3 shows a schematic of the light path in a Kerr microscope. First, the light passes through a polarizer, becoming linearly polarized. It is then focused by the objective lens on the sample surface and subsequently reflected. A portion of this reflected light is filtered by an analyzer and finally, the intensity of the light is detected by a CMOS camera, creating an optical image of the sample. The Kerr rotation manifests itself as contrast variations

in the image intensity.
In order to maximize the contrast, an image subtraction processing was applied to the recorded data presented in this work, thus allowing real-time observation of the magnetic state of the sample. This procedure involves initially saturating the magnetization of the sample in the out-of-plane direction ($\pm\hat{u}_z$) and then saving the image captured by the camera. Afterwards, this background image is subtracted from the recorded frames during the process under investigation.

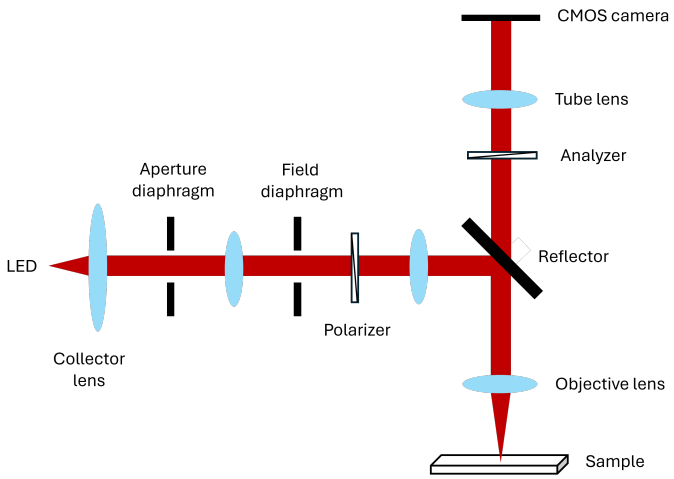

Figure 3.3: Schematic of the Kerr microscope showing the path of the light propagating towards the sample. Adapted from [13].

Chapter 4

Device characterization

A significant part of the current research in spintronics is focused on current-driven motion of 180° domain walls, boundaries between two magnetic domains where the magnetization in one domain points in the opposite direction with respect to the magnetization in the adjacent domain. However, the group Integnano has recently demonstrated the existence of 90° domain walls in magneto-ionic devices where a spin reorientation transition is induced by the gate voltage [8]. In this chapter, the characterization of this new spin structure will be addressed.

4.1 Device description and experimental setup

Due to the time constraints and the safety training required for cleanroom facilities at C2N, the fabrication of the device was carried out by Guillaume Bernard, a PhD student in the group. The main steps are summarized below. The all-solid-state device under study is an heterostructure consisting of Ta(5 nm)/$Co_{20}Fe_{60}B_{20}$(1 nm)/HfO_2 (3 nm) thin films grown by magnetron sputtering on a thermally oxidized silicon substrate with a thickness of 100 nm. The materials were deposited and provided by Singulus Technologies in Germany. The HfO_2 capping layer prevents the oxidation of the ferromagnetic material (CoFeB) which otherwise would have been in contact with air. This specific magnetic material was chosen for its technological relevance in CoFeB/MgO based tunneling junctions. An additional layer of HfO_2 (20 nm) was grown by atomic layer deposition (ALD) on top of the film stack. Finally, a 100 nm thick indium tin oxide (ITO) is used as the counter electrode. The thickness was chosen to have an optimal compromise between transparency and conductivity, enabling the observation of magnetic textures. Additionally, the wavelength of the light source illuminating the device, to which the stack must be transparent, was another important factor to consider. A graphic representation of the device is presented in Figure 4.1a (right inset).
As discussed in Section 3.1, when a current is injected into a ferromagnet with magnetization M, the anomalous Hall effect leads to the generation of a voltage drop perpendicular to both. The geometric configuration sketched in Fig.4.1b, known as Hall bar, is able to detect this voltage drop by injecting a bias current of 100 μA in one arm and measuring the Hall voltage across the perpendicular one. The width of the Hall bars range from 5 μm

to 40 μm. The latter width was the one used for all the measurements conducted at room temperature and presented in this report. Moreover, the magnetic field perpendicular to the sample is generated by means of a solenoidal electromagnet placed underneath the sample.

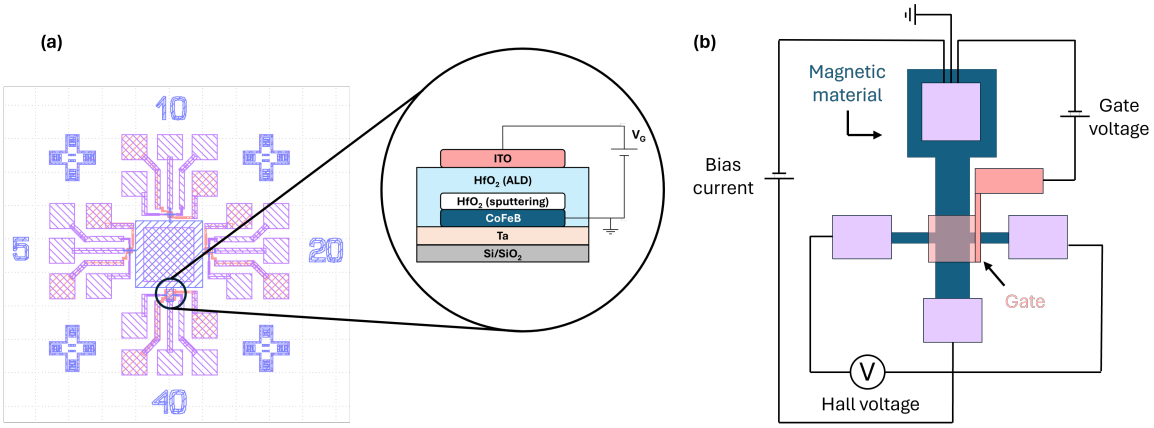

Figure 4.1: (a) Graphic representation of the Hall bars ranging from 5 μm to 40 μm. The right inset shows the magneto-ionic device under study. (b) Schematics of the device geometry for transport measurements.

4.2 Magneto-transport measurements with pulsed gate voltage

The key characteristic of any ferromagnetic material is its non-linear response of magnetization M to an applied magnetic field H, known as magnetic hysteresis. Therefore, in order to obtain an initial characterization of the device under study, a hysteresis loop was recorded by gradually sweeping the magnetic field from zero to positive saturation, then to a negative saturation, and back to positive before returning to zero. The vertical component of the magnetization can be detected experimentally by means of the Hall voltage as a function of the applied magnetic field perpendicular to the device, as shown in Figure 4.2. The square-shaped loop (purple curve) reflects a magnetization process along an easy axis. This indicates that the as-grown device exhibits perpendicular magnetic anisotropy (PMA), a state in which the easy axis of magnetization is perpendicular to the sample and therefore parallel to the magnetic field. Unlike previous results from the Integnano group [10], here the initial under-oxidized IPA state was not found, supposedly due to the additional fabrication step involving the 20 nm layer of HfO_2 grown by ALD. Furthermore, the irreversibility of the IPA $\rightarrow$ PMA transition (regime I) prevented us to reach this state.

Upon applying negative voltage pulses with constant amplitude and width (V_p = -6V, t_p = 3s, Δt = 1s), the remanence decreased significantly as a result of the oxygen ion migration towards the CoFeB layer, while the coercive field seems not to be affected, as can be seen in Figure 4.2 (magenta curve). The easy axis of the system gradually changed from out-of-plane to in-plane. The small remanent hysteresis cycle indicates that there is

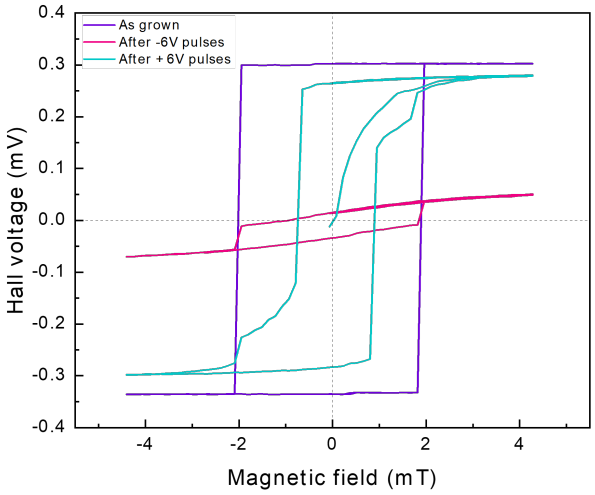

Figure 4.2: Hysteresis cycles of the as-grown state (purple curve) after cumulative negative voltage pulses (magenta curve) and after sequential positive voltage pulses (light blue curve).

still a PMA component that adds to the total Hall voltage. This may likely be related to the magnetization of the ungated Hall cross leads which were used in the transport measurements. The electrical signal highlights the fact that the spin-reorientation transition occures only under the gated area. In order to verify whether the gating effects were reversible, we applied positive voltage pulses (V_p = 6V, t_p = 3s, Δt = 1s). The gate driven motion of the oxygen ions away from the surface of the CoFeB thin film allows only a partial recovery of the initial PMA state (light blue curve). The small steps before the magnetization switching corresponding to the ungated area are still present, while the remanence increased. Nevertheless, it is possible that this partial switching of anisotropy could also occur beneath the gated area, potentially due to an insufficient applied voltage to restore the system to the initial state. This asymmetric behaviour of gate pulses of the same amplitude and width confirmed the presence of different mechanisms at play, being oxidation from PMA to IPA and reduction from IPA to PMA. Different energy barriers are associated to the two chemical processes. Thus, higher voltages has been applied to further force the system into PMA for subsequent measurements.

In order to get a deeper understanding of the anisotropy changes in the device, the hysteresis loops were correlated to transport measurements based on the anomalous Hall effect and to images taken in real time with a Kerr microscope. After the initial hysteresis loop was taken to determine the magnetic state of the device, cumulative negative gate pulses (V_p = -6V, t_p = 3s, Δt = 1s) were applied to the sample at zero magnetic field. It is important to point out that the measured Hall voltage and the Kerr images were taken simultaneously after each gate pulse. The acquisition of the former took $\sim$ 100 ms, while almost 1 s for the latter. In Figure 4.3, three arbitrary images per different gate

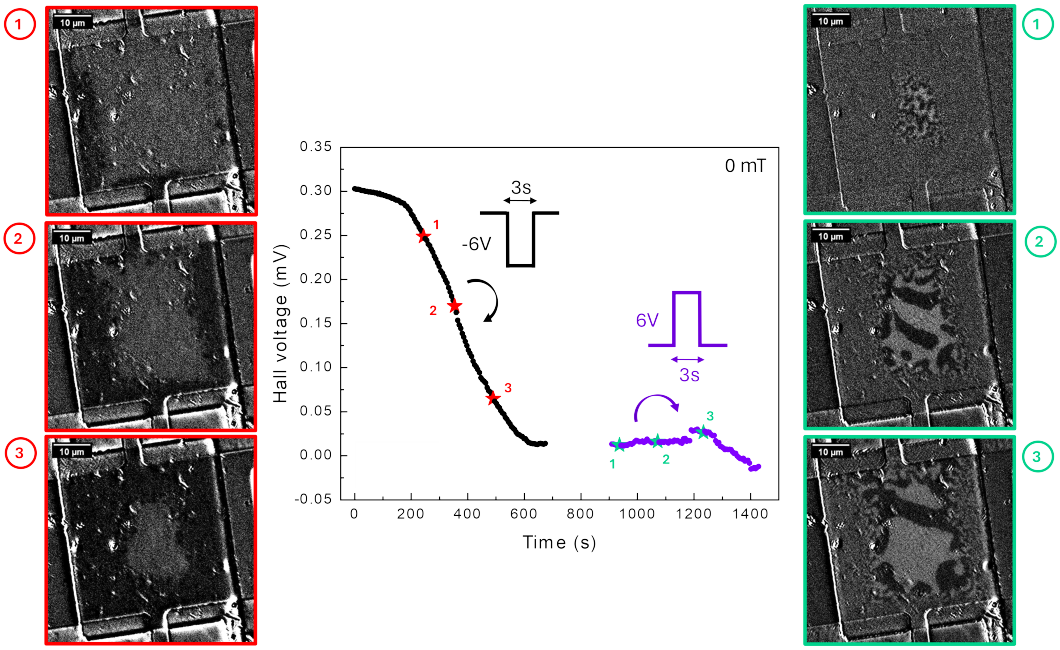

Figure 4.3: Transport measurements of the Hall voltage as a function of time with no magnetic field applied. Each data point corresponds to the measured Hall voltage after one gate pulse, being either negative or positive. The left and right insets show the Kerr images of the device after the 45th, 65th and 90th negative pulse and after the 5th, 30th and 60th positive pulse, respectively. A spin reorientation transition is observed.

pulse polarity are shown to better appreciate the changes in the anisotropy state. It is evident that the transition from PMA to IPA is not homogeneous. Instead, a 90° domain wall ($DW_{\Updownarrow\Longleftrightarrow}$) between the two anisotropy states appears and propagates from the edges of the sample towards the centre, as we can see from the different insets on the left. As the DW moves through the magnetic film, the anisotropy axis changes direction from out-of-plane to in-plane and the Hall voltage decreases up to a saturation point. This data point coincides with the DW reaching the centre of the device. On the other hand, a completely different behaviour was observed with positive gate pulses of same amplitude and width. Although the hysteresis loop taken after the sequential positive pulses showed a transition from IPA to PMA, the Hall voltage seemed not to react to the gate. By looking at the Kerr images after positive cumulative pulses (right insets of Figure 4.3), multiple magnetic domains originate at the centre and progressively propagate towards the edges of the sample. By gradually progressing towards PMA, the magnetization does not have a preferred out-of-plane direction until a perpendicular magnetic field is applied. Furthermore, the magnetic dipoles arising at the sample surface will result in an unstable system due to the high demagnetizing field associated with the out-of-plane magnetization. One way for the system to minimize its total energy is through the formation of magnetic domains with opposite spin direction ($\uparrow$, $\downarrow$). This behaviour accounts for the electric signal observed in the AHE measurements: the spin-up and spin-down domains cancel each other out leading to an almost zero net magnetization which corresponds to an almost zero Hall voltage. As we can see from the right insets of Fig. 4.3, the DW does not reach the edge of

the sample, confirming that the hysteresis loop recorded after the positive voltage pulses in Fig. 4.2 is linked to the partial switching between the two anisotropy states under the gated area. On the other hand, the transition from PMA to IPA does not exhibit the same multi-domain configuration, but we cannot have access to further information because polar Kerr microscopy is not sensitive to the in-plane component of the magnetization.

It became clear that obtaining a signal from the reverse process (IPA $\rightarrow$ PMA) required a magnetic field. Figure 4.4*a* shows the same measurement discussed previously, but performed with $\mu_0 H = 0.5$ mT. As predicted, the magnetic images did not feature any magnetic domains for the IPA $\rightarrow$ PMA transition (purple curve). Indeed, a sufficiently large magnetic field was able to align the magnetization along the perpendicular easy axis, parallel to the direction of the applied field. As a consequence, the Hall voltage increases upon applying positive gate pulses. Considering the analogy with memristors, the weight of our magnetic synapse could be encoded in the anomalous Hall resistance, which is proportional to the net out-of-plane magnetization. Within this picture, different values of this resistance correspond to the different weights of the magnetic synapse.

The same experimental procedure was employed for the following measurements, shown in Fig. 4.4, with the only difference being the pulse amplitude. Negative gate pulses (V_p = -6V, V_p = -7V, V_p = -8V t_p = 3s, Δt = 1s) and positive gate pulses (V_p = +6V, V_p = +7V, V_p = +8V t_p = 3s, Δt = 1s) were applied to induce the transition of the device from PMA to IPA and from IPA to PMA, respectively. The device is exposed to the same perpendicular magnetic field of 0.5 mT. As presented in Fig. 4.5, increasing the amplitude of the pulses from 6V to 8V leads to a faster reorientation of the easy axis for both transitions. However, the time evolution of the magnetic anisotropy is different: more than twice the time is needed to drive the system back to a PMA state starting from IPA compared to the opposite transition.

On a parallel line, Fig. 4.6 shows the hysteresis cycles corresponding to different states of the sample before and after the pulses for several pulse amplitudes. Once again V_p = +6V and V_p = +7V failed to bring the system back to the initial oxidized state, suggesting that the reduction process at the interface of the CoFeB layer exhibits a higher energy barrier than the oxidation. Interestingly, the hysteresis loops acquired after V_p = +8V revealed that the initial saturated PMA state is recovered, as shown in Fig. 4.6c. Hence, a higher voltage is required to drive the system back to the optimally oxidized state.

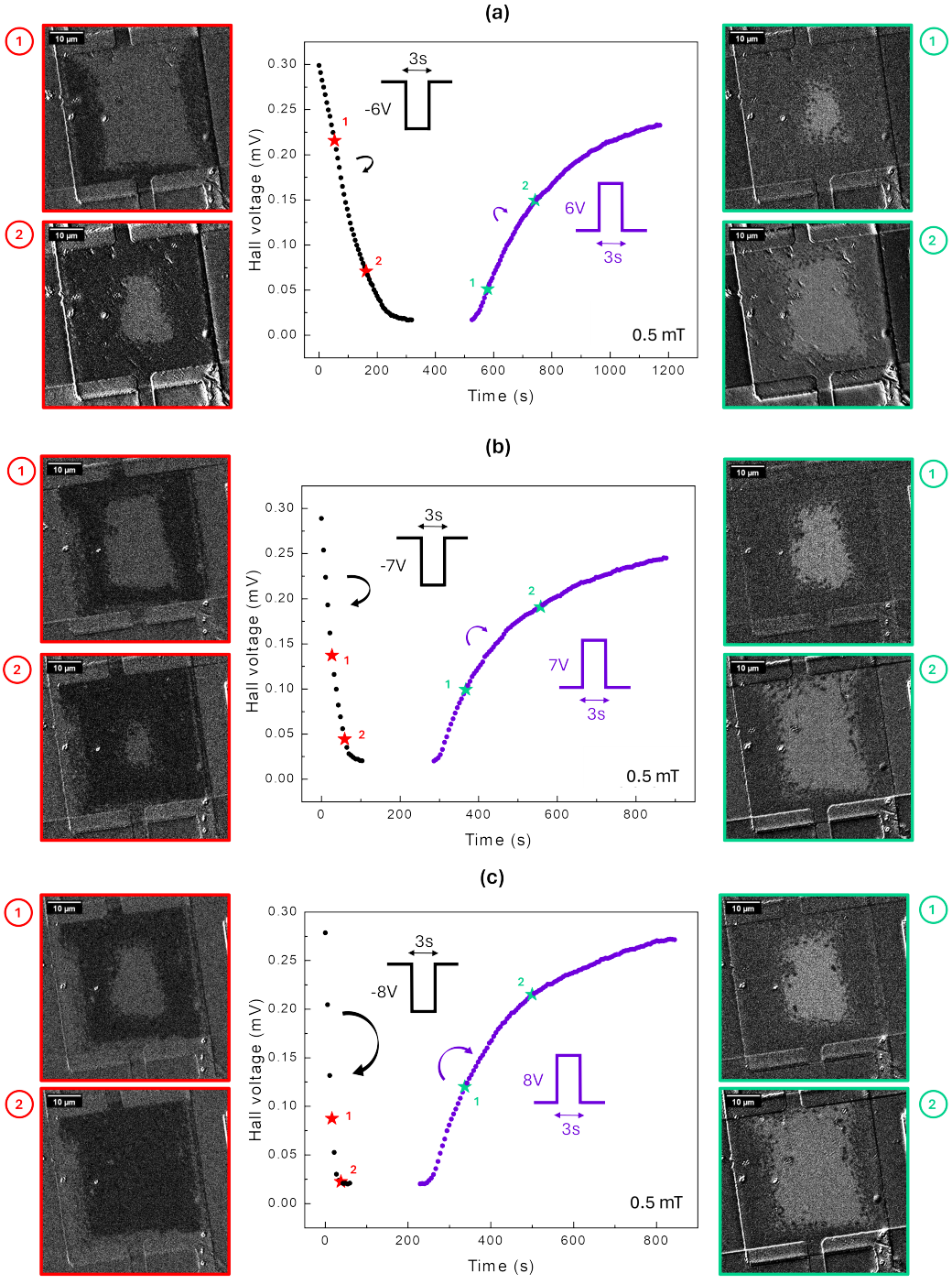

Figure 4.4: Transport measurements showing the evolution of the Hall voltage over time under (a) V_p = -/+ 6V, (b) V_p = -/+ 7V, (c) V_p = -/+ 8V, t_p = 3s, Δt = 1s and the corresponding Kerr images taken through the transparent ITO gate. A magnetic field of 0.5 mT is applied.

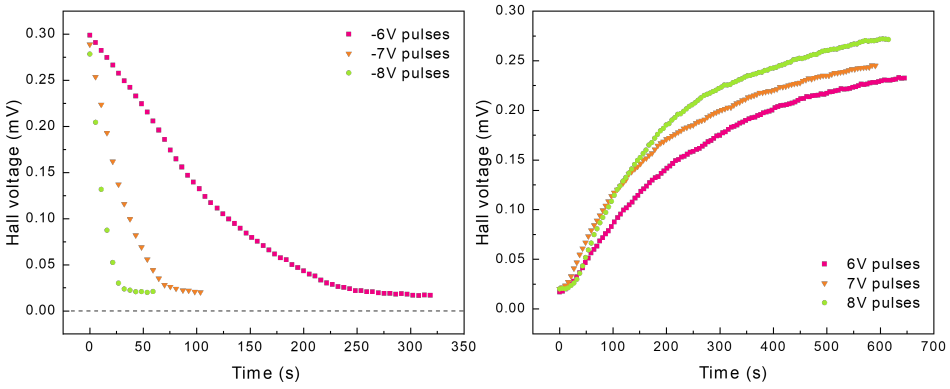

Figure 4.5: Comparison of the Hall voltage over time between different gate pulses amplitudes of same polarity. Higher gate voltages have a distinct effect on the redox process.

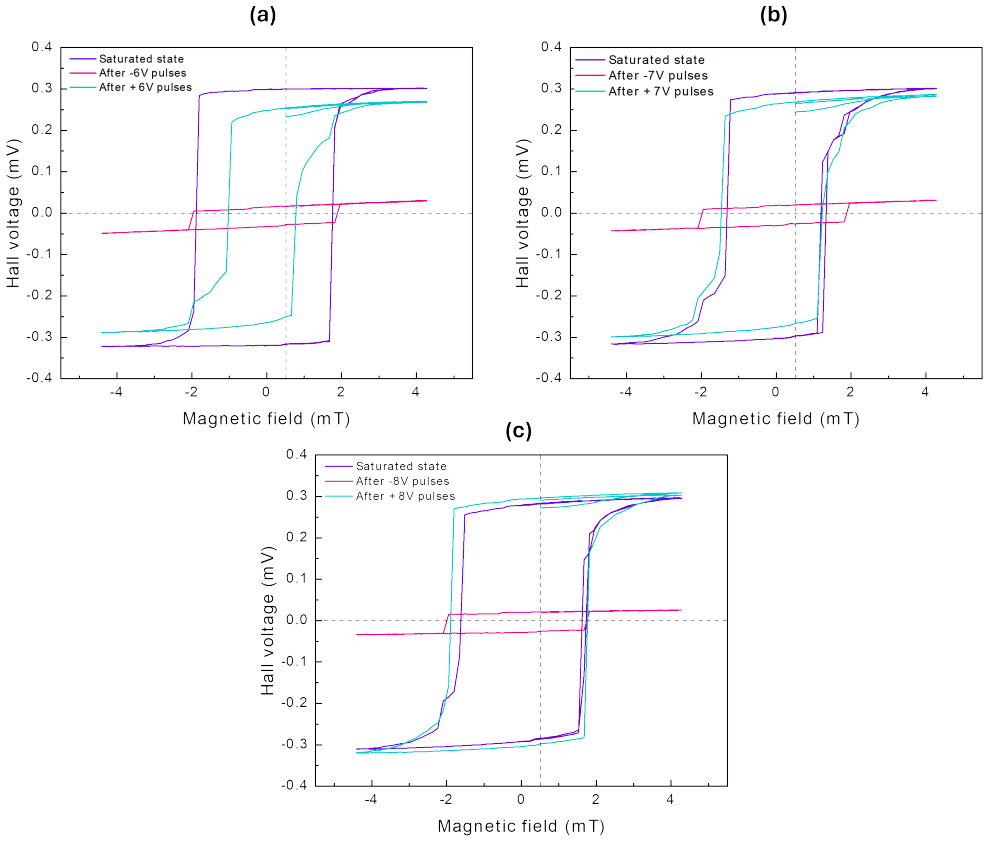

Figure 4.6: Different hysteresis cycles of the saturated state, after cumulative negative voltage pulses (V_p = -6V, V_p = -7V, V_p = -8V, t_p = 3s, Δt = 1s) and after sequential positive voltage pulses (V_p = +6V, V_p = +7V, V_p = +8V, t_p = 3s, Δt = 1s). The vertical dashed lines represent the magnetic field (0.5 mT) applied for the transport measurements.

4.3 90° domain wall motion

The gate-driven motion of 90° domain walls (DW) between the two anisotropy states (PMA and IPA) can be analyzed as the effects of the gate voltages are non-volatile. Image subtraction processing was employed to evaluate the DW displacement as a function of the cumulative gating time. Kerr microscopy images of 90° domain walls subjected to the tenth and the thirtieth pulse of amplitude -6V are shown in Fig.4.7, as an example. An ideal region (red rectangle) was identified where the domain walls travel in a straight line from one edge of the gated area to the centre. We assumed that the main source of uncertainty of the DW position is its width, given the fact that the boundaries of the 90° domain walls are not sharp. Consequently, an error of ± 3 pixels was estimated. Figure 4.8 shows the DW displacement from the left and right edge as a function of the cumulative gating time under different negative gate pulses. After few pulses the position of the domain walls exhibits, in first approximation, a linear behaviour with respect to the gating time. Note that in Fig.4.8a and Fig.4.8b, the data points representing the DW position before the seventh and second pulse, respectively, were purposely not considered in the mean velocity calculation. The ion dynamics likely requires some build-up time to reach a steady regime. As displayed in Fig.4.9, the extracted mean DW velocities increase with higher gate voltage, resulting in a faster dynamics.

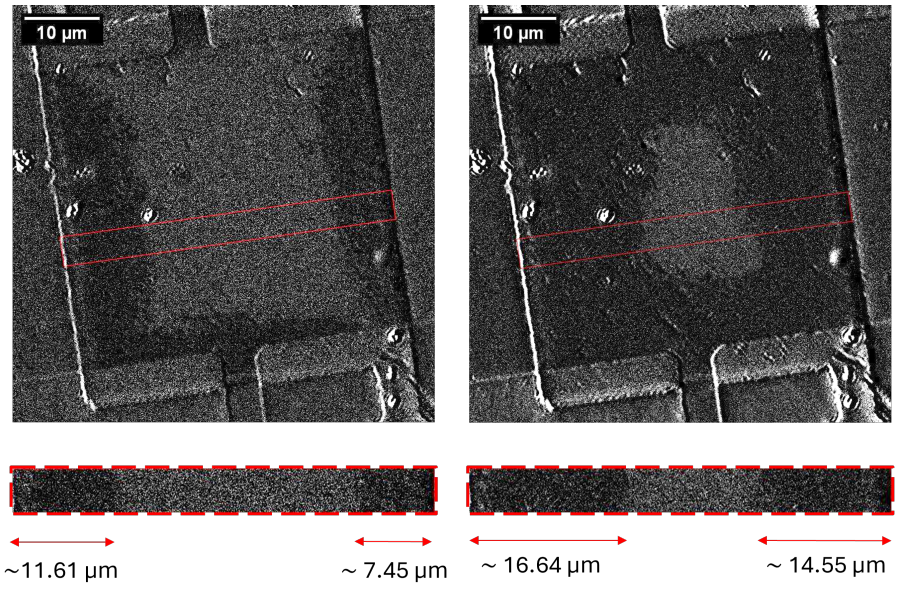

Figure 4.7: Kerr microscopy images of the domain walls displacement after the tenth and thirtieth negative pulse (V_p = -6V, t_p = 3s), showing a spin reorientation transition between PMA (light area) and IP anisotropy (dark area) state. The bottom insets show an enlargement of the area (red rectangle) used for all the domain wall motion measurements. The scale 12.6 pixel/μm was set.

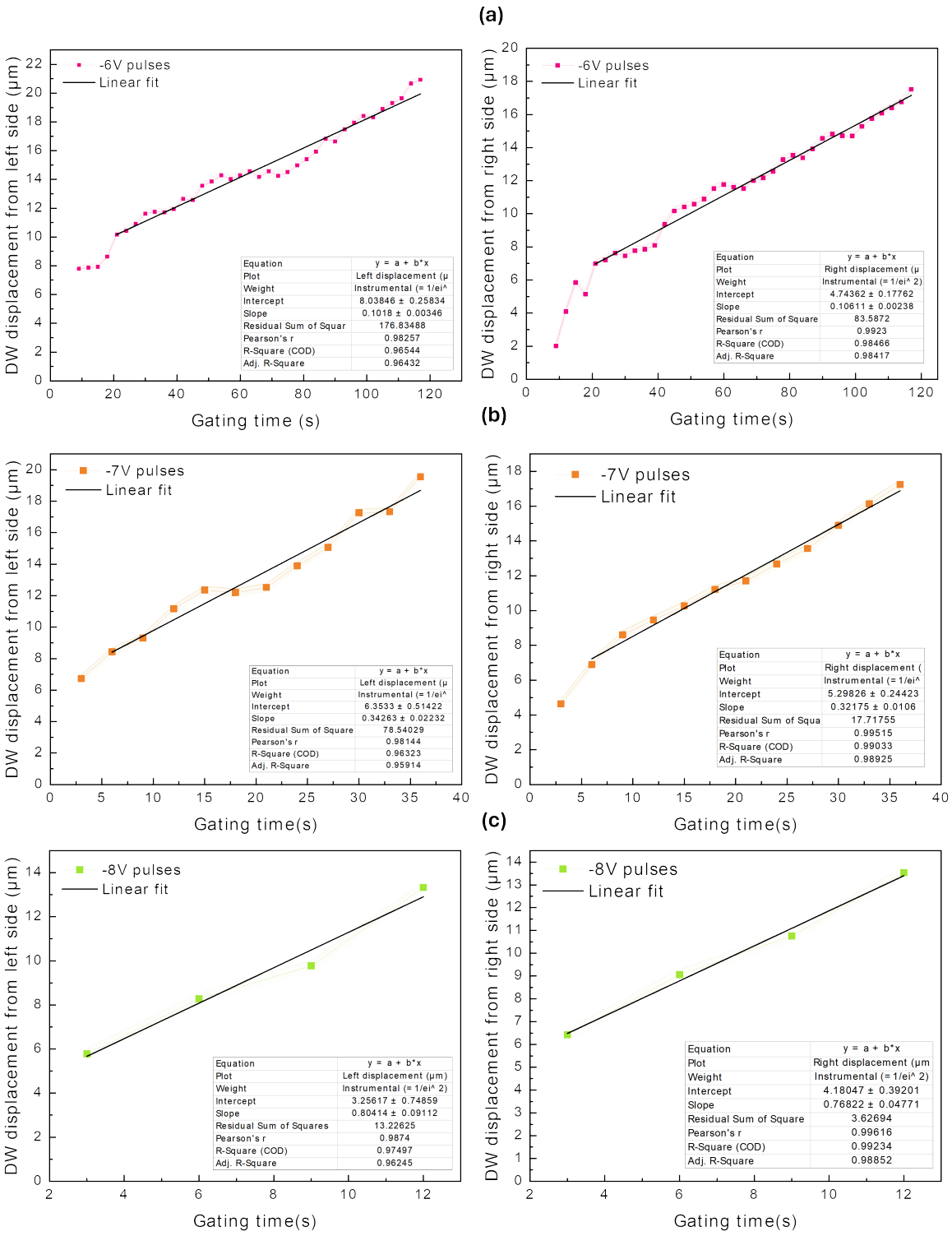

Figure 4.8: Domain wall displacement from the left side and right side of the gated area as a function of the cumulative gating time for (a) V_p = -6V, (b) V_p = -7V, (c) V_p = -8V, t_p = 3s, Δt = 1s and the corresponding linear fits. The shaded area represents the error bar taken into account.

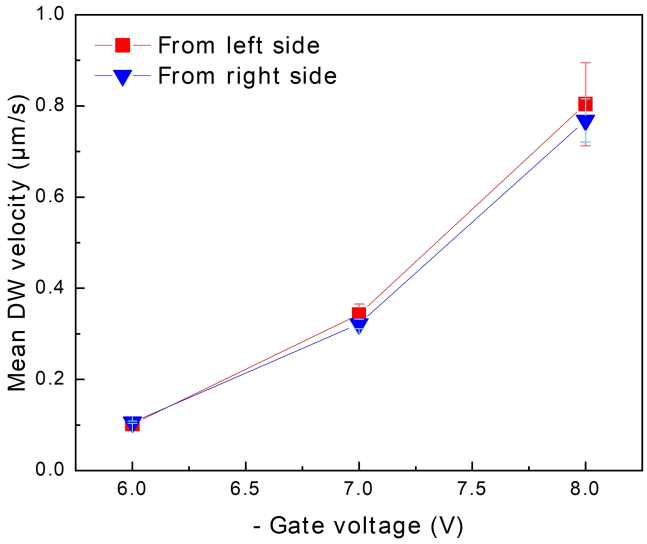

Figure 4.9: Mean DW velocity as a function of negative gate pulses for the DW propagating from the left and from the right edge of the device. The two domain walls move with almost the same velocity.

Chapter 5

Conclusions

Dynamic control of magnetism through electric fields has emerged as a promising approach to manipulate magnetic states, without the need for traditional current-induced methods. In this study, magnetic anisotropy was effectively tuned by the gate voltage, as demonstrated by the reversible transition between PMA and IPA states shown in the hysteresis loops. Nevertheless, the reversibility of the transition depends on the degree of oxidation at the interface between the magnetic film and the oxide, as the oxygen ions dynamics is hindered by different energy barriers. Transport measurements showed that the AHE voltage can be modulated in a non-volatile way through cumulative gate voltage pulses, emulating the behaviour of potentiation and depression of artificial synapses. Additionally, Kerr microscopy magnetic imaging unveiled that the gate-voltage induced spin-reorientation transition occurs through the propagation of a 90° magnetic domain wall between two magnetic anisotropy regions, a spin structure that has never been manipulated before. This, however, limited the comparison with other experimental results.

Since its motion was characterized under a relatively long pulse width, the following step would be understanding the domain wall dynamics under a wide range of different and shorter gate voltage pulses which is essential to assess its ability to replicate synaptic functionalities. Intuitively, a threshold value beyond which the pulse width is too short to trigger any movement of the oxygen ions is expected. Furthermore, the reproducibility of the gate voltage effects across numerous cycles should also be addressed.

References

[1] S. Monso, B. Rodmacq, S. Auffret, G. Casali, F. Fettar, B. Gilles, B. Dieny, P. Boyer. "Crossover from in-plane to perpendicular anisotropy in Pt/CoFe/AlOx sandwiches as a function of Al oxidation: A very accurate control of the oxidation of tunnel barriers". *Applied Physics Letters* 80.22, June 2002, pp. 4157–4159. https://doi.org/10.1063/1.1483122

[2] B. Dieny and M. Chshiev. "Perpendicular magnetic anisotropy at transition metal/oxide interfaces and applications". *Reviews of Modern Physics* 89.2, June 2017, p. 025008. https://doi.org/10.1103/RevModPhys.89.025008

[3] A. Manchon, C. Ducruet, L. Lombard, S. Auffret, B. Rodmacq, B. Dieny, S. Pizzini, J. Vogel, V. Uhlíř, M. Hochstrasser, G. Panaccione."Analysis of oxygen induced anisotropy crossover in Pt/Co/MOx trilayers". *Journal of Applied Physics* 104.4, August 2008, p. 043914. https://doi.org/10.1063/1.2969711

[4] L. Herrera Diez, D. Chiba, D. A. Gilbert, S. Granville, K. Leistner. "Magneto-ionic and electrostatic gating of magnetism: Phenomena and devices". *Applied Physics Letters* 123.13, September 2023, p. 130401. https://doi.org/10.1063/5.0176639

[5] U. Bauer, L. Yao, A. Tan et al. "Magneto-ionic control of interfacial magnetism". *Nature Materials* 14.2, 2015, pp. 174–181. https://doi.org/10.1038/nmat4134

[6] A.J. Tan, M. Huang, C.O. Avci et al. "Magneto-ionic control of magnetism using a solid-state proton pump". *Nature Materials* 18.1, 2019, pp. 35–41. https://doi.org/10.1038/s41563-018-0211-5

[7] J. de Rojas, A. Quintana, A. Lopeandía et al. "Voltage-driven motion of nitrogen ions: a new paradigm for magneto-ionics". *Nature Communications* 11.1, 2020, p. 5871. https://doi.org/10.1038/s41467-020-19758-x

[8] Tristan da Câmara Santa Clara Gomes and Tanvi Bhatnagar-Schöffmann, et al. "Control of the magnetic anisotropy in multirepeat Pt/Co/Al heterostructures using magnetoionic gating", *Physical Review Applied* 21.2, February 2024, p. 024010. https://doi.org/10.1103/PhysRevApplied.21.024010

[9] T. Bhatnagar-Schöffmann, A. Kovàcs, R. Pachat, et al. "Controlling interface anisotropy in CoFeB/MgO/HfO2 using dusting layers and magneto-ionic gating".

Applied Physics Letters 122.4, January 2023, p. 042402. https://doi.org/10.1063/5.0132870

[10] R. Pachat, D. Ourdani, J.W. van der Jagt, et al. "Multiple Magnetoionic Regimes in $Ta/Co_{20}Fe_{60}B_{20}/HfO_2$". *Physical Review Applied* 15.6, June 2021, p. 064055. https://doi.org/10.1103/PhysRevApplied.15.064055

[11] D. Strukov, G. Snider, D. Stewart et al. "The missing memristor found". *Nature* 453, 2008, pp. 80–83. https://doi.org/10.1038/nature06932

[12] Naoto Nagaosa, Jairo Sinova, Shigeki Onoda, A. H. MacDonald, and N. P. Ong. "Anomalous Hall effect". *Reviews of Modern Physics* 82.2, May 2010, pp. 1539–1592. https://doi.org/10.1103/RevModPhys.82.1539

[13] Rohit Pachat, "Magneto-ionics in CoFeB based systems". PhD Thesis. Université Paris-Saclay, February 2023. http://www.theses.fr/2023UPAST032